J Mater Sci (2009) 44:3364–3369
DOI 10.1007/s10853-009-3439-2

Hydrothermal synthesis and luminescence properties of core-shell-structured PS@$SrCO_3$:Tb^{3+} spherical particles

Y. Y. Zhang · J. L. Liu · Y. X. Zhu · Y. Shang · M. Yu · X. Huang

Received: 30 November 2008 / Accepted: 24 March 2009 / Published online: 16 April 2009

Abstract Nanocrystalline $SrCO_3$:Tb^{3+} phosphor layers were coated on monodisperse and spherical polystyrene particles by a typical hydrothermal synthesis without further annealing treatment, resulting in the formation of core-shell-structured polystyrene@$SrCO_3$:Tb^{3+} particles. X-ray diffraction, field emission scanning electron microscopy, transmission electron microscopy, photoluminescence, as well as lifetimes were employed to characterize the resulting composite particles. Under ultraviolet excitation, the polystyrene@$SrCO_3$:Tb^{3+} phosphors show the characteristic $^5D_4$–^7F_J (J = 6, 5, 4, 3) emission lines with green emission $^5D_4$–$^7F_5$ (544 nm) as the most prominent group. The obtained core-shell phosphors are potentially applied in fluorescent lamps.

Introduction

Nanometer- and micrometer-sized core-shell-structured particles with special physical and chemical properties have attracted great attention due to their potential applications in photonic crystals, catalysis, diagnostics, and pharmacology [1–5], as well as the ability to fine-tune their properties [6–11]. Core-shell materials consist of a core structural domain covered by a shell domain, both of which may be composed of a variety of materials, including polymers, inorganic solids, and metals. In general, the preparation of core-shell structures involves surface modification of particles, often accomplished by coating or encapsulating them with a different material that has desired properties. So far, considerable kinds of core-shell structures have been designed and fabricated, including semiconductor/semiconductor [12], semiconductor/dielectric [13], metal/dielectric [14], metal/semiconductor [15], inorganic particle/polymer, polymer or inorganic particle/biomolecule [1], etc. The structure, size, and composition of these particles can be easily altered in a controllable way to tailor their magnetic, optical, mechanical, thermal, electrical, electro-optical, and catalytic properties. A variety of approaches have been employed in the manufacture of the core-shell-structured materials, such as layer-by-layer self-assembly [1, 8, 10], co-precipitation [16–18], surface reaction [19], sol–gel process [20–23], MOCVD [24], etc. However, the controlled coating of particles with homogeneous and organized layers without causing aggregation remains a challenge for the scientists.

Strontium carbonate ($SrCO_3$) is a very important industrial reagent in the production of glass for color television picture tubes and ferrite magnets for small DC motors [25]. $SrCO_3$ is also widely used in the production of iridescent and special glasses, driers, paints, pyrotechnics, and chemical sensor. Several methods for the preparation of $SrCO_3$ (micro/nanostructures) have been previously reported such as the refluxing process [26], ion entrapment methods [27], biological synthesis using the fungus *Fusarium oxysporum* [28], catalytic decomposition [29], and self-assembled monolayers [30–33], but these still suffer from complex and expensive procedure. Comparatively, the hydrothermal process is an effective and versatile route for the synthesis of materials in terms of low-cost, high efficiency, and good potential for high-quantity production [34–37].

Y. Y. Zhang · J. L. Liu · Y. X. Zhu · Y. Shang · M. Yu (✉) · X. Huang
College of Chemistry, Northeast Normal University, Changchun 130024, People's Republic of China
e-mail: yum406@nenu.edu.cn

Polystyrene (PS) can be fabricated controllably into spherical morphology, being frequently used in core-shell-structured materials [38, 39], as a core or a shell. If the polystyrene spheres are coated with phosphor layers, kinds of core-shell phosphor materials with spherical morphology will be obtained. The core-shell phosphor materials will be cheaper than the pure phosphor materials.

Herein, we developed a typical hydrothermal synthesis to obtain monodisperse and spherical core-shell-structured PS@$SrCO_3$:Tb^{3+}, and the structure, morphology, photoluminescent properties of the resulting samples were characterized in detail.

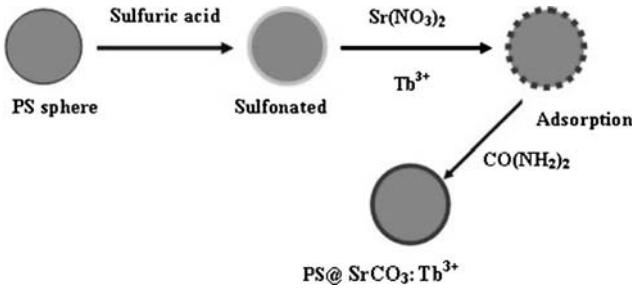

Scheme 1 The formation mechanism of PS@$SrCO_3$:Tb^{3+} composite microspheres

Experimental

Preparation of monodisperse PS and sulphonated PS microspheres

All of the reagents and solvents were analytical grade and used without further purification. Monodisperse PS microspheres were prepared by dispersion polymerization method [40, 41]. To prepare sulfonated PS microspheres, PS fine powder (1.7 g) was dispersed into 60 mL concentrated sulfuric acid (98%) by ultrasonication. Then the sulfonation took place at 40 °C under magnetic stirring for 12 h. The products were collected by centrifugation and washed with absolute ethanol several times. Finally, the sample was dried in vacuum at 60 °C.

Coating of $SrCO_3$:Tb^{3+} phosphor layers on the PS particles to obtain the core-shell-structured PS@$SrCO_3$:Tb^{3+} particles

The typical procedure is as follows: firstly, terbium oxide (99.99%) was dissolved in dilute nitric acid HNO_3 (A.R., Beijing Beihua Chemicals Co., Ltd.) under vigorous stirring, then the solution was evaporated to eliminate the superfluous HNO_3. The mole ratio of Tb^{3+} to Sr^{2+} ranges from 2% to 10%. After being cooled to room temperature, the as-obtained sample was dissolved in a water–ethylene glycol (EG) (A.R., Beijing Fine Chemical Company, China) (v/v = 1:24) solution to form terbium nitrate solution. Secondly, 0.15 g sulfonated PS microspheres were added into the terbium nitrate solution with ultrasonication for 30 min. Subsequently, 2 mmol $Sr(NO_3)_2$ and 2 g $(NH_2)_2CO$ (A.R., Beijing Fine Chemical company, China), were introduced slowly, and the mixture was kept stirring for 3 h. Then the mixture was transferred into a 50 mL Teflon-lined stainless autoclave and heated at 180 °C for 18 h. After cooling to room temperature naturally, the products were separated by filtration, washed with ethanol (A.R., Beijing Fine Chemical Company, China) and distilled water several times, and dried in air at 100 °C for 8 h. The above process was repeated several times to increase the thickness of the $SrCO_3$:Tb^{3+} shell on the PS surface. The whole experimental process is shown in Scheme 1. When PS template particles were sulfonated with concentrated sulfuric acid, the surface of the sulfonated PS microspheres exhibited a negative charge property. After the introduction of Sr^{2+} and Tb^{3+}, the Sr^{2+} and Tb^{3+} ions were absorbed on the surface of the sulfonated PS, and then the urea was added. The synthesis reactions can be simply expressed as

$$(NH_2)_2CO + H_2O \rightarrow CO_2 + NH_3 \quad (1)$$

$$Sr^{2+} + CO_2 + H_2O \rightarrow SrCO_3 + 2H^+ \quad (2)$$

Under the hydrothermal process, the decomposition of urea at elevated temperatures produces CO_2 and NH_3 firstly, as described in reaction (1). Then Sr^{2+} reacts with CO_2 and H_2O to produce the final products $SrCO_3$, as described in reaction (2).

Characterization

The samples were characterized by powder X-ray diffraction (XRD) on a Rigaku-Dmax 2500 diffractometer with Cu Kα radiation ($\lambda = 0.15405$ nm). The morphology of the samples was inspected using a field emission scanning electron microscope (FESEM, XL 30, Philips) and a transmission electron microscope (TEM, JEOL-2010, 200 kV). Photoluminescence (PL) excitation and emission spectra were recorded with a Hitachi F-4500 spectrophotometer equipped with a 150 W Xenon lamp as the excitation source. The luminescence decay curve were obtained from a Lecroy Wave Runner 6100 Digital Oscilloscope (1 GHz) using a tunable laser (pulse width = 4 ns, gate = 50 ns) as the excitation (Contimuum Sunlite OPO). All the measurements were performed at room temperature.

Results and discussion

Structure and morphology

Typical TEM and SEM images of the PS (Fig. 1a, c) and sulfonated PS (Fig. 1b, d) microspheres are showed in Fig. 1. It can be seen that the PS particles have a non-agglomeration spherical morphology with a diameter of about 2.1 μm, and good monodisperse, but sulfonated PS particles are slightly smaller than pure PS particles, and show a little deviation in size distribution.

Figure 2 shows the XRD profiles for the sulfonated PS (a), pure $SrCO_3$:Tb^{3+} (b) power samples, and the core-shell-structured PS@$SrCO_3$:Tb^{3+} (c) through the hydrothermal process, respectively. For sulfonated PS particles (Fig. 2a), no diffraction peak is observed except for a broad band centered at $2\theta = 18.95°$. For PS@$SrCO_3$:Tb^{3+} core-shell particles without annealing (Fig. 2c), all the diffraction peaks can be indexed according to the standard data of $SrCO_3$ (JCPDS 74-1491). This agrees well with the pure $SrCO_3$ power sample. No additional peaks of other phases have been found, indicating that Tb^{3+} has been effectively built into the host lattice. In general, the nanocrystallite size can be estimated from the Scherrer formula: $D_{hkl} = K\lambda/(\beta\cos\theta)$, where λ is the X-ray wavelength (0.15405 nm), β is the full-width at half-maximum, θ is the diffraction angle, K is a constant (0.89), and D_{hkl} is the size along the (hkl) direction [30]. Here we take diffraction data along the (111) plane at $2\theta = 25.09°$ to calculate the size of the nanocrystallites, and the estimated average crystallite sizes of $SrCO_3$:Tb^{3+} are 36.37 nm for $SrCO_3$:Tb^{3+} on the sulfonated PS spheres and also that of the pure $SrCO_3$:Tb^{3+} powders are around 29.64 nm.

FESEM and TEM

Figure 3 shows the FESEM micrographs of the sulfonated PS particles (a) and sulfonated PS particles coated by one layer $SrCO_3$:Tb^{3+} (b), (c). From the FESEM micrograph of Fig. 3a, we can observe that the sulfonated spherical PS particles with an average size of 2.2 μm, and these particles are non-aggregated with narrow size distribution. After the PS particles by $SrCO_3$:Tb^{3+} coatings, the resulting PS@$SrCO_3$:Tb^{3+} particles still keep the spherical properties of the PS, i.e., these particles are still spherical, but rougher than the sulfonated PS particles due to the additional layer of $SrCO_3$:Tb^{3+} on them, as shown in Fig. 3b and c. This indicates that all of $SrCO_3$:Tb^{3+} materials have been coated on the surfaces of PS particles by our experimental process. To investigate the detailed structure of PS@$SrCO_3$:Tb^{3+} core-shell samples, TEM was performed. Figure 3d shows the PS particles coated by $SrCO_3$:Tb^{3+} layer. The core-shell structure for the PS@$SrCO_3$:Tb^{3+} particles can be seen clearly due to the different electron penetrability for the cores and shells, and the particle size is

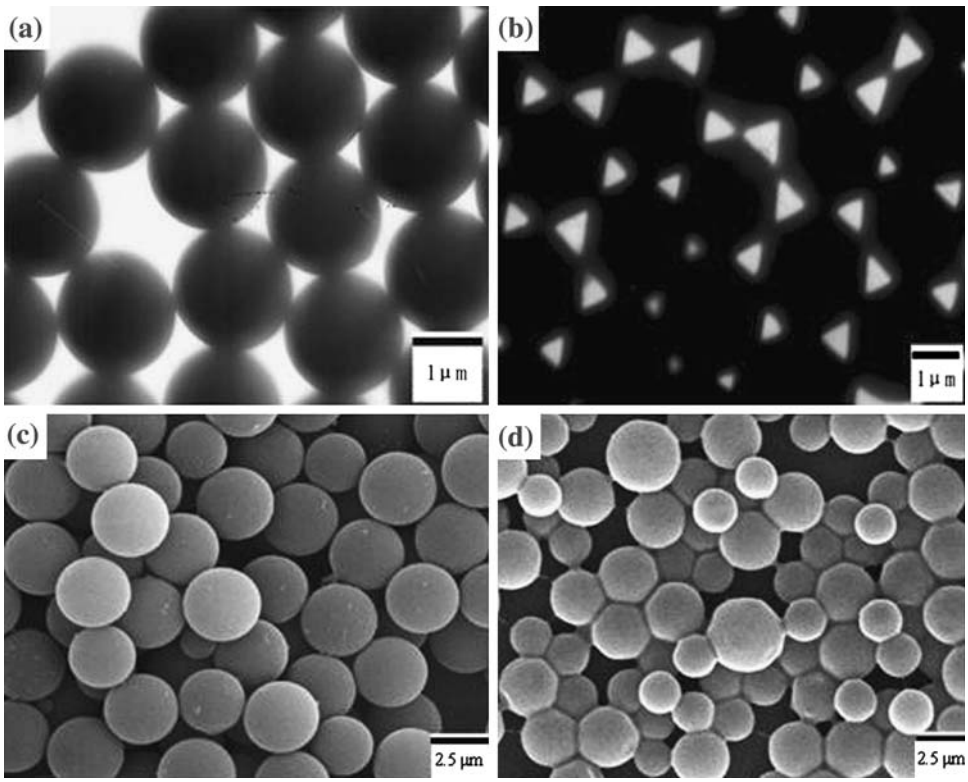

Fig. 1 TEM and SEM images of monodisperse PS (**a**, **c**) and sulfonated PS (**b**, **d**) microspheres

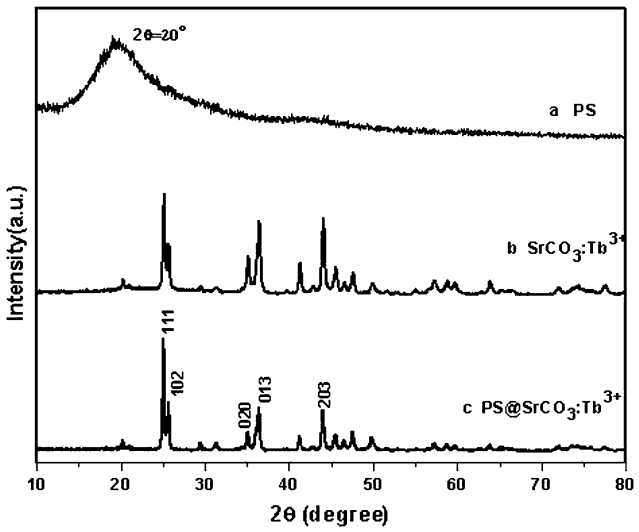

Fig. 2 XRD pattern of PS (**a**) and $SrCO_3$:Tb^{3+} (**b**) as well as the PS@$SrCO_3$:Tb^{3+} core-shell particles (**c**)

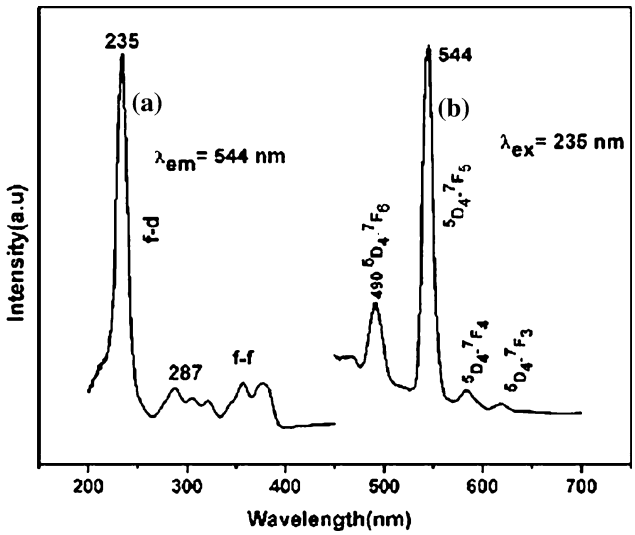

Fig. 4 Excitation (**a**) and emission (**b**) spectra of PS@$SrCO_3$:Tb^{3+} core-shell particles

larger than that of sulfonated PS cores, which indicates that the thickness of coating is about 20–40 nm.

Photoluminescence properties

The PS@$SrCO_3$:Tb^{3+} core-shell particles exhibit a strong green emission under short ultraviolet (235 nm) excitation spectrum due to the f–d transitions of Tb^{3+} in $SrCO_3$ lattice. Figure 4 shows the excitation (a) and emission (b) spectra of PS@$SrCO_3$:Tb^{3+} core-shell phosphors. The excitation spectrum contains an intense, broad band from 200 to 350 nm with a maximum at 235 nm due to the spin-allowed $4f^8$–$4f^7$5d transitions ($\Delta S = 0$) of Tb^{3+}. The ground states ($4f^8$) of the Tb^{3+} are $7F_J$ configurations. When one electron is promoted to 5d, it gives rise to two $4f^7 5d^1$ excitation states: the high-spin state with $9D_J$ configurations or low-spin state with $7D_J$ configurations. Obviously, $9D_J$ states will be lower in energy according to the Hund's rule, and the transitions between $7F_J$ and $7D_J$ are spin-allowed, while the transitions between $7F_J$ and $9D_J$ are spin-forbidden.

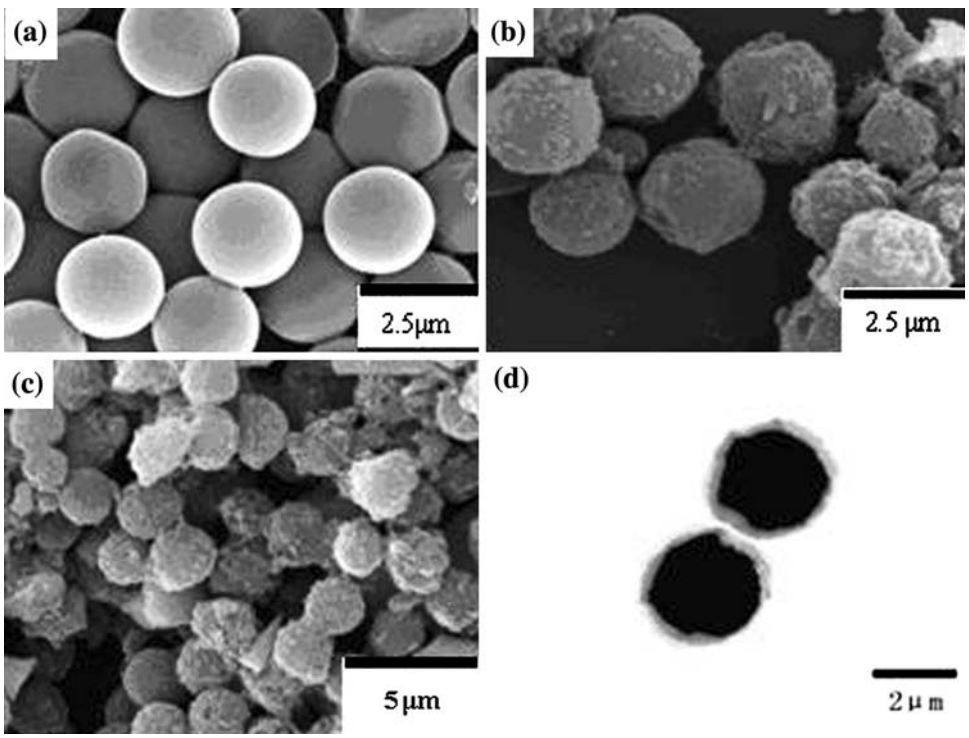

Fig. 3 FESEM micrographs of the as-formed PS (**a**), the PS particles coated with one layer of $SrCO_3$:Tb^{3+} (**b**, **c**), as well as the TEM micrograph (**d**) for the particles in (**b**)

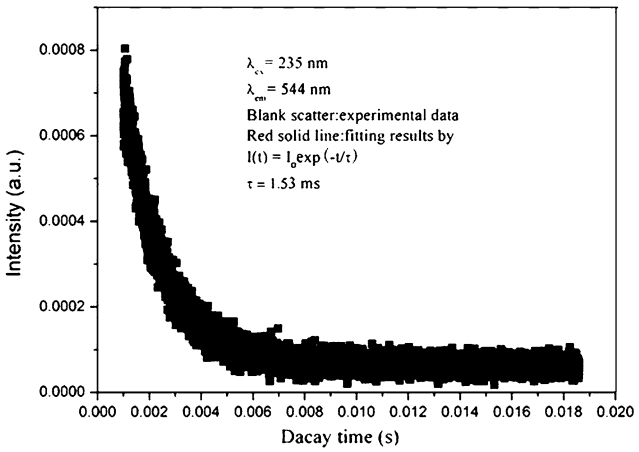

Fig. 5 Decay curve for the $^5D_4$-$^7F_5$ (544 nm) emission of Tb^{3+} in PS@$SrCO_3$:Tb^{3+}core-shell samples

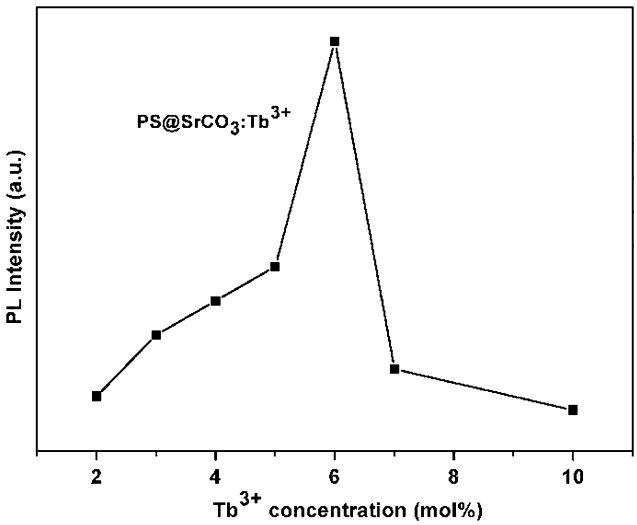

Fig. 6 PL emission intensities of Tb^{3+} as function of its concentration in PS@$SrCO_3$:Tb^{3+} samples

Therefore, Tb^{3+} in a specific host exhibits two groups of f–d transitions: The spin-allowed f–d transitions are strong, with higher energy; the spin-forbidden f–d transitions are weak, with lower energy, corresponding to 235 and 287 nm in $SrCO_3$ host, respectively. The excitation lines in the longer wavelength regions can be seen at this magnification with weak intensity, which is from spin-forbidden component of $4f^8$–$4f^7$5d transitions ($\Delta S = 1$). Upon excitation at the spin-allowed $4f^8$–$4f^7$5d transitions at 235 nm, the obtained emission spectra consist of f–f transition lines within Tb^{3+} $4f^8$ electron configuration, i.e., $^5D_4$–$^7F_6$ (490 nm) in the blue region and $^5D_4$–$^7F_5$ (544 nm) in the green region, as well as $^5D_4$–$^7F_4$ (583 nm), $^5D_4$–$^7F_3$ (618 nm) in the red region, respectively. The strongest one is located at 544 nm corresponding to $^5D_4$–$^7F_5$ of Tb^{3+}. Due to the cross-relaxation between $^5D_3$–$^5D_4$ and $^7F_0$–$^7F_6$, and the existing of impurities such as OH, -OR, H_2O, NO_3^-, the blue emission of $^5D_3$–^7F_J transition is quenched. Figure 5 shows the luminescence decay curve of the PS@$SrCO_3$:Tb^{3+}core-shell samples. The decay curve for $^5D_4$–$^7F_5$ (544 nm) of Tb^{3+} can be well fitted into a single exponential function as $I = I_0 \exp(-t/\tau)$, in which I_0 is the initial emission intensity at $t = 0$, and τ is the 1/*e* lifetime of the emission center. The lifetime of Tb^{3+} (544 nm) in PS@$SrCO_3$:Tb^{3+} core-shell samples is determined to be 1.53 ms. The luminescence provides us an additional proof that the as-formed products are not a mixture of $SrCO_3$ and $Tb_2(CO_3)_3$, but that Tb^{3+} ions have successfully entered the host crystal lattice as activators under the hydrothermal process.

Tuning the PL emission intensity

(a) Concentration effect

By varying the contents of Tb^{3+} ion in $SrCO_3$ host, we determined the optimum compositions with the highest emission intensity. Figure 6 shows the dependence of the PL emission intensity of Tb^{3+} on its doping concentration in PS@$SrCO_3$:Tb^{3+} core-shell phosphors. The PL emission intensity of Tb^{3+} increased firstly, reached a maximum value at 6 mol%, and then decreased with increasing Tb^{3+} concentration due to the concentration quenching. Thus the optimum doping concentration for Tb^{3+} green emission is 6% of Sr^{2+} in $SrCO_3$ host. As can be seen, the intensity of the emission decreases with increasing Tb^{3+} concentration due to cross-relaxation. In Tb^{3+}, the energy gap between the $^5D_3$ and $^5D_4$ levels is close to that between the $^7F_6$ and $^7F_0$ levels. As a result, if the Tb^{3+} concentration is sufficiently high, the higher energy level emission can be easily quenched in favor of the lower energy level emission.

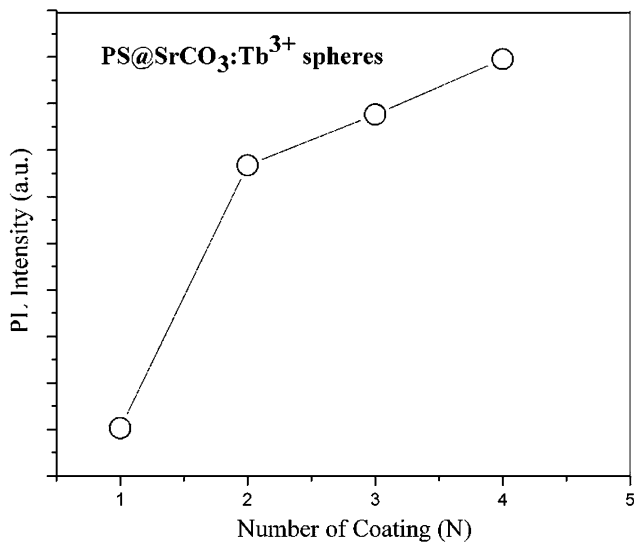

Fig. 7 The PL emission intensity of PS@$SrCO_3$:Tb^{3+} sample as a function of the number of coating (*N*)

(b) Number of coatings (N) effect

The number of the coating (*N*) is also an important factor influencing PL intensity. Figure 7 shows the effect of coating number (i.e., the number of layers) on the PL intensity of PS@$SrCO_3$:Tb^{3+} core-shell phosphors. The PL intensity increases with increasing coating number, which is due to the increase of the thickness of $SrCO_3$:Tb^{3+} shells on the PS spheres. When the coating is 4, the PL intensity of core-shell phosphors is about 70% of that of pure $SrCO_3$:Tb^{3+} powders excited at a wavelength of 235 nm.

Conclusion

Micrometer PS@ $SrCO_3$:Tb^{3+} core-shell particles were prepared by an effective and simple hydrothermal synthesis process without further annealing. The obtained PS@$SrCO_3$:Tb^{3+} core-shell phosphors maintain the spherical morphology and narrow size-distribution of the originals. Under ultraviolet excitation, phosphors show strong green emission corresponding to $^5D_4$–$^7F_5$ (544 nm) of Tb^{3+}, the optimum concentration for Tb^{3+} was determined to be 6 mol% of Sr^{2+} in $SrCO_3$ host. Furthermore, the PL intensity of the core-shell phosphors can be tuned by the number of coatings. The emission intensity of the phosphors increased as the number of coatings was increased. Adequate reaction time is necessary to obtain high PL intensity.

Acknowledgement This project is financially supported by the Training Fund of NENU'S Scientific Innovation Project (NENU-STC07014).

References

1. Schartl W (2000) Adv Mater 12:1899
2. Caruso F (2001) Adv Mater 13:11
3. Suryanarayanan V, Nair AS, Tom RT (2004) J Mater Chem 14:2661
4. Oldenberg SJ, Averitt RD, Westcott SL, Halas NJ (1998) Chem Phys Lett 288:243
5. LizMarzan LM, Giersig M, Mulvaney P (1996) Langmuir 12:4329
6. Lu Y, Yin Y, Li ZY, Xia Y (2002) Nano Lett 2:785
7. Caruso RA, Antonietti M (2001) Chem Mater 13:3272
8. Schuetzand P, Caruso F (2002) Chem Mater 14:4509
9. Hall SR, Davis SA, Mann S (2000) Langmuir 16:1454
10. Salgueirino-Maceira V, Spasova M, Farle M (2005) Adv Funct Mater 15:1036
11. Liu S, Han M (2005) Adv Funct Mater 15:961
12. Peng XG, Schlamp MC, Kadacanich AV, Alicisatos AP (1997) J Am Chem Soc 119:7019
13. Wilson WL, Szajowski PF, Brus LE (1993) Science 262:1242
14. Hardikar VV, Matijevic′ E (2000) J Colloid Interface Sci 221:133
15. Lei Y, Chim WK (2005) J Am Chem Soc 127:1487
16. Giesche H, Matijevic′ E (1994) J Mater Res 9:436
17. Liu GX, Hong GY (2005) J Solid State Chem 178:1647
18. Ocana M, Gonzalez-Elipe AR (1999) Colloid Surf A 157:315
19. Dokoutchaev A, James JT, Koene SC, Pathak S, Prakash GKS, Thompson ME (1999) Chem Mater 11:2389
20. Yu M, Lin J, Fang J (2005) Chem Mater 17:1783
21. Wang H, Lin CK, Liu XM, Lin J, Yu M (2005) Appl Phys Lett 87:181907
22. Yu M, Wang H, Lin CK, Li GZ, Lin J (2006) Nanotechnology 17:3245
23. Wang H, Yu M, Lin CK, Liu XM, Lin J (2007) J Phys Chem C 111:11223
24. Chang KW, Wu JJ (2005) Adv Mater 17:241
25. Bastow TJ (2002) Chem Phys Lett 354:156
26. Du JM, Liu ZM, Li ZH, Han BX, Huang Y, Zhang JL (2005) Microporous Mesoporous Mater 83:145
27. Rautaray D, Sainkar SR, Sastry M (2003) Langmuir 19:888
28. Rautaray D, Sanyal A, Adyanthaya SD, Ahmad A, Sastry M (2004) Langmuir 20:6827
29. Sondi I, Matijevic E (2003) Chem Mater 15:1322
30. Aizenberg J, Black AJ, Whitesides GM (1999) J Am Chem Soc 121:4500
31. Küther J, Bartz M, Seshadri R, Vaughane GBM, Tremela W (2001) J Mater Chem 11:503
32. Küther J, Nelles G, Seshadri R, Schaub M, Butt HJ, Tremela W (1998) Chem Eur J 4:1834
33. Küther J, Seshadri R, Tremela W (1998) Angew Chem Int Ed 37:3044
34. Cao MH, Wu XL, He XY, Hu CG (2005) Langmuir 21:6093
35. Li SZ, Zhang H, Xu J, Yang DR (2005) Mater Lett 59:420
36. Huang Q, Gao L, Cai Y, Aldinger F (2004) Chem Lett 33:290
37. Yang J, Liu XM, Li CX, Quan ZW, Kong DY, Lin J (2007) J Cryst Growth 303:480
38. Yang Y, Chu Y, Zhang Y, Yang F (2006) J Solid State Chem 179:470
39. Zhang YP, Chu Y, Yang Y (2007) Colloid Polym Sci 285:1061
40. Paine A, Luymes W, McNulty J (1990) Macromolecules 23:3104
41. Yang Y, Chu Y, Yang F, Zhang Y (2005) Mater Chem Phys 92:164